CFA-4: a fluorinated metal–organic framework with exchangeable interchannel cations

J. Fritzsche, M. Grzywa, Dmytro Denysenko, V. Bon, I. Senkovska, S. Kaskel, Dirk Volkmer

Angaben zur Veröffentlichung / Publication details:

Fritzsche, J., M. Grzywa, Dmytro Denysenko, V. Bon, I. Senkovska, S. Kaskel, and Dirk Volkmer. 2017. "CFA-4: a fluorinated metal–organic framework with exchangeable interchannel cations." *Dalton Transactions* 46 (20): 6745–55. https://doi.org/10.1039/c7dt00582b.

CFA-4 – a fluorinated metal–organic framework with exchangeable interchannel cations†

J. Fritzsche,[a] M. Grzywa,[a] D. Denysenko,[a] V. Bon,[b] I. Senkovska,[b] S. Kaskel[b] and D. Volkmer *[a]

The syntheses and crystal structures of the fluorinated linker 1,4-bis(3,5-bis(trifluoromethyl)-*1H*-pyrazole-4-yl)benzene (H_2-tfpb; **1**) and the novel metal–organic framework family **M[CFA-4]** (Coordination Framework Augsburg University-4), $M[Cu_5(tfpb)_3]$ (M = Cu(I), K, Cs, Ca(0.5)), are described. The ligand **1** is fully characterized by single crystal X-ray diffraction, photoluminescence-, NMR-, IR spectroscopy, and mass spectrometry. The copper(I)-containing MOF crystallizes in the hexagonal crystal system within the chiral space group $P6_322$ (no. 182) and the unit cell parameters are as follows: a = 23.630(5) Å, c = 41.390(5) Å, V = 20 015(6) Å^3. **M[CFA-4]** features a porous 3-D structure constructed from pentanuclear copper(I) secondary building units $\{Cu^I_5(pz)_6\}^-$ (pz = pyrazolate). **Cu(I)[CFA-4]** is fully characterized by synchrotron single crystal X-ray diffraction, thermogravimetric analysis, variable temperature powder X-ray diffraction, IR spectroscopy, photoluminescence and gas sorption measurements. Moreover, thermal stability and gas sorption properties of **K[CFA-4]** and **Cu(I)[CFA-4]** are compared.

Introduction

Porous and crystalline coordination polymers, *i.e.* metal–organic frameworks (MOFs), have attracted the interest of the scientific community during the past 20 years. Whereas at the beginning the focus was laid upon applications in gas storage,[1] these materials later on were tested for a wide range of different applications, such as drug delivery,[2] sensing,[3] gas separation[4] and catalysis.[5]

Replacing hydrogen atoms by fluorine atoms in a MOF-structure leads to so-called FMOFs (fluorous metal–organic frameworks), as published in 2007 for the first time.[6]

Compared to structurally analogous compounds lacking fluorine substituents, FMOFs with fluoro-lined or fluoro-coated channels or cavities are expected to possess an enhanced thermal and chemical stability, hydrophobicity and stability against (self-) oxidation and photolytic decomposition.[7] Furthermore, FMOFs show unique properties such as superacidity, low surface energy and surface tension and excellent optical properties such as persistent luminescence.[8] Owing to the strong hydrophobicity, carboxylate-based FMOFs become water-resistant. In 2015, MOFF-5, a superhydrophobic material with high porosity and an accessible surface area of 2445 m^2 g^{-1}, that shows a high capacity for the storage of fluorinated greenhouse gases (up to 225 wt% for perfluorohexane), was announced.[9]

The number as well as the position of introduced fluorine atoms have huge influence on the behaviour of the structure. The FMOFs TKL-104-TKL-107, for instance, show an increased stability as well as high surface areas and excellent ability for H_2 storage and CO_2 capture, that makes them applicable in energy storage and environment improvement.[10] Another example that demonstrates the influence of the number of fluorous moieties has recently been published as UiO-66-type FMOFs.[11] In UiO-66-F and UiO-66-CF_3 a positive effect of fluorine substitution on the oxygen adsorption capacity was observed. The authors suppose that fluorine atoms have a positive interaction with oxygen, but not with nitrogen.

Besides the capture and storage of (chloro-)fluorocarbons, MOFs find application in photochemistry,[12] as electroluminescent displays and chemical sensors,[13] biosensors[14] and fluorescent sensors.[15] The basic principle of fluorescence-based sensing is, that these materials show a “turn-on” or “turn-off” behaviour, when a special analyte is introduced in the system. This works for gases,[16] ions,[17] pesticides[18] as well as for explosives. The latter materials are often highly electron-deficient nitrated organic compounds that act as good electron accep-

[a]*Augsburg University, Institute of Physics, Chair of Solid State and Materials Chemistry, Universitaetsstrasse 1, 86159 Augsburg, Germany. E-mail: dirk.volkmer@physik.uni-augsburg.de; Fax: +49 (0)821 598 5955; Tel: +49 (0)821598 3006*

[b]*Department of Inorganic Chemistry, Dresden University of Technology, Bergstrasse 66, 01062 Dresden, Germany*

†Electronic supplementary information (ESI) available: Crystallographic data and topology analysis, NMR-, IR-, UV-Vis-, mass- and photoluminescence spectra, gas sorption measurements, EDX, TGA and VTXRPD data for **CFA-4**. CCDC 1532600 and 1532837. For ESI and crystallographic data in CIF or other electronic format see DOI: 10.1039/c7dt00582b

tors leading to a fluorescence quenching of a MOF, and thus allowing their specific detection.

For applications of MOFs in gas separation or sensing it is important that the sample is stable and has a high volumetric density of uniform active sites. Small molecules as for example carbon monoxide can bind reversibly at low temperatures and can be easily removed again.

We showed this in previous works on **CFA-8**[19] and **CFA-9**,[20] that contain Cu(I) sites which are able to reversibly bind carbon monoxide. We further published **Cu^{I}-MFU-4*l***,[21] a representative of the **MFU-4** family, that is highly robust against thermal and hydrolytic decomposition and contains highly reactive, threefold-coordinated unsaturated open Cu(I)–metal centres. **Cu^{I}-MFU-4*l*** shows fully reversible chemisorption of small molecules such as O_2, N_2 or H_2 with high isosteric heats of adsorption as well as strong binding of carbon monoxide. This leads to the supposition, that introduction of unsaturated Cu(I) sites into a MOF could be a promising approach towards materials suitable for gas separation or sensing applications as well as for catalytic applications.

We here report on the synthesis and structure of a new copper(I)-based MOF family **M[CFA-4]**, which is synthesized from the fluorinated organic ligand 1,4-bis(3,5-bis(trifluoromethyl)-1*H*-pyrazole-4-yl)benzene (H_2-tfpb; **1**). The H_2-tfpb ligand was successfully synthesized *via* a twofold Suzuki-coupling reaction. Its crystal structure was determined by single crystal X-ray structure analysis. In addition to the synchrotron single crystal X-ray diffraction, **Cu(I)[CFA-4]** was characterized by thermogravimetric analyses, variable temperature X-ray diffraction, IR spectroscopy, photoluminescence and gas sorption measurements. Moreover, thermal stability and porosity of **K[CFA-4]** and **Cu(I)[CFA-4]** are compared to each other.

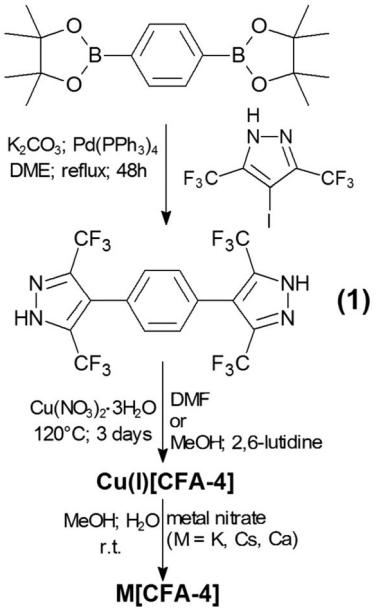

Scheme 1 Syntheses of 1,4-bis(3,5-bis(trifluoromethyl)-1*H*-pyrazole-4-yl)benzene **1**, **Cu(I)[CFA-4]** and **M[CFA-4]** (DME = 1,2-dimethoxyethane).

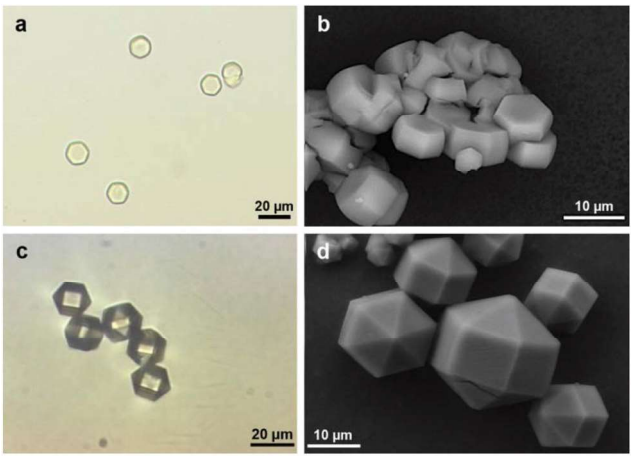

Fig. 1 **Cu(I)[CFA-4]**: (a) optical micrograph after synthesis in DMF as solvent; (b) SEM image after synthesis in DMF as solvent; (c) optical micrograph after synthesis with solvent methanol and 2,6-lutidine; (d) SEM image after synthesis with solvent methanol and 2,6-lutidine.

Results and discussion

Syntheses and characterization

1,4-Bis(3,5-bis(trifluoromethyl)-1*H*-pyrazole-4-yl)benzene (H_2-tfpb; **1**) was synthesized in a twofold Suzuki-coupling reaction of commercially available 1,4-bis(4,4,5,5-tetramethyl-1,3,2-dioxaborolan-2-yl)benzene with 4-iodo-3,5-bis(trifluoromethyl)-1*H*-pyrazole[22] (Scheme 1).

Cu(I)[CFA-4] framework was obtained as hexagonal prisms (Fig. 1a and b) after heating a DMF solution of **1** and copper(II) nitrate trihydrate at 120 °C (Scheme 1). In a different synthetic approach, a solution of **1** and copper(II) nitrate trihydrate were heated in MeOH in the presence of 2,6-lutidine, where hexagonal prismatic-bipyramidal crystals of **Cu(I)[CFA-4]** were obtained (Fig. 1c and d).

Substituted **M[CFA-4]** frameworks (M^{n+} = K^+, Cs^+, Ca^{2+}) were obtained *via* postsynthetic cation exchange reactions upon treatment of **Cu(I)[CFA-4]** with a solution of the corresponding metal nitrate in a DMF/H_2O mixture at room temperature. Detailed reaction information is shown in the experimental part. The Cu/M molar ratios in the obtained products were determined by energy dispersive X-ray spectroscopy (EDX) and correspond well to the expected theoretical values (5 : 1 for singly charged cations K^+ and Cs^+ and 10 : 1 for a doubly charged cation Ca^{2+}, see ESI Fig. S18–S20; Table S3†). XRPD patterns of metal exchanged **M[CFA-4]** frameworks show similar peak positions as **Cu(I)[CFA-4]** (see ESI Fig. S12 and 13†).

Crystal structure analyses

1,4-Bis(3,5-bis(trifluoromethyl)-1*H*-pyrazole-4-yl)benzene·2MeOH (H_2-tfpb·2MeOH; $C_{16}H_6F_{12}N_4{\cdot}2CH_3OH$). **1**·2MeOH crystallizes in the monoclinic crystal system within the space group *C*2/*m*

(no. 12). Detailed description of the crystal structure of H_2-tfpb·2MeOH is presented in the ESI (Fig. S1 and S2, Table S1†).

Cu(I)[Cu_5(tfpb)$_3$]·4.75DMF (Cu(I)[CFA-4])

A synchrotron single crystal X-ray diffraction study reveals that **Cu(I)[CFA-4]** crystallizes in the hexagonal crystal system in the chiral space group $P6_322$ (no. 182).

The asymmetric unit consists of five copper atoms and one and a half of the tfpb^{2-} molecules (Fig. 2).

Cu(I)[CFA-4] features a 3-D porous framework structure constructed from pentanuclear $\{Cu^{I}_5(pz)_6\}^-$ secondary building units (SBUs). Within the $\{Cu^{I}_5(pz)_6\}^-$ SBU, five Cu(I) ions are connected by twelve nitrogen atoms belonging to the pyrazolate moieties of tfpb^{2-} ligands. The pentanuclear copper(I) unit, Cu_5N_{12} are composed of two distorted trigonal-planar coordinated copper centres, Cu3 and Cu5, and three linearly twofold-coordinated copper(I) ions, Cu4 (Cu2) and Cu1. For the twofold-coordinated atoms, the N–Cu–N angles range from 177.84(11) to 179.87(13)°, whereas the Cu–N distances are in the range of 1.860(2) to 1.891(2) Å. The Cu–N distances for trigonal-planar coordinated copper ions range from 1.948(2) to 1.979(2) Å. These values are similar to those observed for the coordination compound $[Et_3NH]^+\{Cu_5[3\text{-}(C_2F_5)IndF_4]_6\}^-$ ([3-(C_2F_5)IndF_4]H = 3-pentafluoroethyl-4,5,6,7-tetrafluoro-1*H*-indazolate) featuring similar pentanuclear Cu(I) coordination units.[23] To the best of our knowledge, **M[CFA-4]** represents the first example of a copper-containing MOF family in which the pentanuclear copper(I) SBU was found and structurally characterized. The $\{Cu^{I}_5(pz)_6\}^-$ SBUs of the **M[CFA-4]** framework are interconnected by benzene rings of tfpb^{2-} ligand, thus creating one-dimensional channels expanding in *c*-direction of the crystal lattice (see Fig. 3d). Taking the van der Waals radii of fluorine atoms (1.35 Å) into account, the narrowest channel diameter calculated between the fluorine atoms of the CF_3-groups is 14.3 Å. The estimation with the program SQUEEZE[24] reveals that the initial solvent accessible void volume is 11 724.2 Å^3 (0.64 cm^3 g^{-1}), which is 58.6% of the unit cell volume (20 015(6) Å^3) for a probe radius of 1.68 Å, corresponding to the approximate van der Waals radius of argon.[25] In the crystal structure of **Cu(I)[CFA-4]** the channels are occupied by disordered DMF molecules and Cu^+-ions, which compensate a negative charge of the lattice. As the UV-Vis spectrum of **Cu(I)[CFA-4]** (see ESI Fig. S31†) shows no typical band for Cu(II), we suppose that there are only Cu^+-ions in the channels. These Cu^+-ions can be readily exchanged by other ions such as alkaline or earth alkaline metal ions, as described in detail in the Experimental part. The positions of the disordered solvent molecules and Cu^+-ions were impossible to resolve and to refine from the electron density distribution. According to the crystallographic data there is an electron count of 1312 per unit cell (rest of the electron density), which corresponds to 6 Cu^+ and 28.5 DMF molecules in the unit cell of **Cu(I)[CFA-4]**. Thus, the composition of the framework is determined as $[Cu_5(tfpb)_3]^-$ (Cu^+)·4.75DMF.

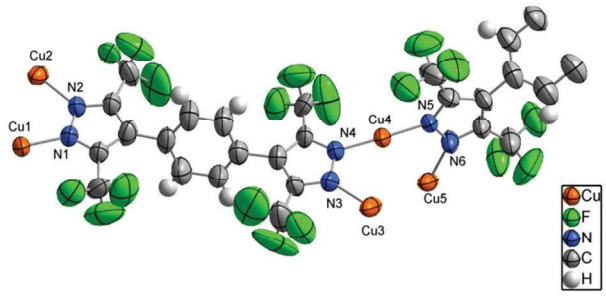

Fig. 2 ORTEP-style plot of the asymmetric unit of **Cu(I)[CFA-4]**. Thermal ellipsoids probability: 50%. Disordered F-atoms were omitted for clarity.

Topology analysis using the TOPOS program[26] (see ESI S3†) reveals a new type of the topology: 2,6-c net with stoichiometry (2-c)3(6-c); 2-nodal net. The chirality of the network results from the symmetry of the SBU (point group symmetry of the SBU: C_3).

Thermal analysis and VTXRPD studies

Thermal and structural stability of **Cu(I)[CFA-4]** and **K[CFA-4]** were determined from TGA and VTXRPD measurements. To remove the occluded solvent molecules, the samples were dried in vacuum at 100 °C for 4 h prior to TG measurements. As shown in Fig. 4, the thermogravimetric profile of **Cu(I)[CFA-4]** (red line) under nitrogen exhibits two weight loss steps. The mass of the sample is constant up to about 180 °C. In the temperature range of 200–300 °C, the weight loss (7.4%) is attributed to the removal of DMF molecules coordinated to the Cu^+ ions in the channels and corresponds to two DMF molecules per one Cu^+ ion (calculated weight loss 7.4%). The next step between 450–800 °C is connected with gradual decomposition of the framework. Compared to **Cu(I)[CFA-4]**, the TGA curve of **K[CFA-4]** (black line) shows no weight loss until about 300 °C indicating that no solvent molecules are coordinated to K^+ ions. Such behavior can be explained by very weak coordinating properties of K^+ ions. Above 300 °C, the framework starts to decompose.

Phase purity of **Cu(I)[CFA-4]** and **K[CFA-4]** was confirmed by XRPD measurements (Fig. 5 and 6, respectively) of samples stored under ambient conditions. The experimental XRPD pattern is consistent with one calculated from the single crystal structural data (see Fig. 5). Differences in peak intensities are due to occluded solvent molecules. Variable temperature X-ray powder diffraction studies of **Cu(I)[CFA-4]** (Fig. 5) are in good agreement with the results from the TGA measurement. The framework is stable up to 150 °C. Above this temperature the intensity of the first peak strongly decreases until it completely disappears at 200 °C. A new crystalline phase of unknown structure is formed that is stable in the temperature range from 250 to 400 °C. The unit cell parameters of the new phase were determined by DICVOL and TREOR 90 program[27] based on the powder pattern collected at 300 °C. Both programs determined a quite similar orthorhombic cell with the cell parameters: a = 16.690 Å, b = 15.997 Å, c = 8.331 Å, V =

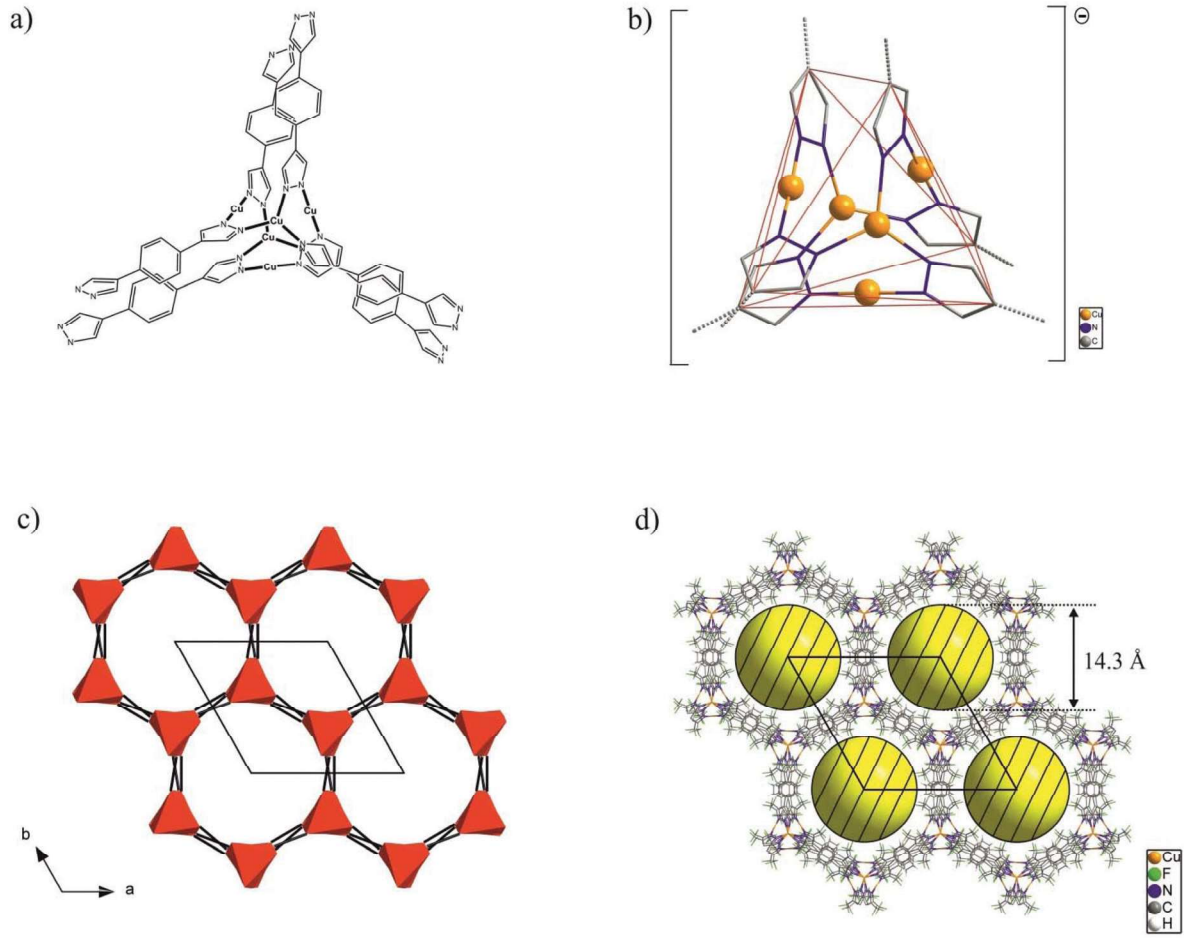

Fig. 3 (a) Excerpt of the coordination framework of **M[CFA-4]** featuring pentanuclear Cu(I) unit. (b) Representation of a single SBU of **M[CFA-4].** CF_3-groups were omitted for clarity. (c) Schematic packing diagram representing interconnected SBUs of **M[CFA-4]**, view in the *c*-direction. (d) Crystal structure of **M[CFA-4]** with channels (represented by yellow spheres), view in the *c*-direction. Disordered CF_3-groups (a–c), solvent molecules and hydrogen atoms (a–c) were omitted for clarity.

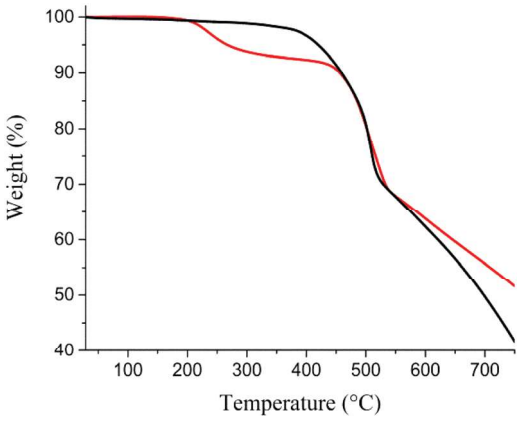

Fig. 4 Temperature dependent weight loss of **Cu(I)[CFA-4]** (red line) and **K[CFA-4]** (black line) under flowing nitrogen gas.

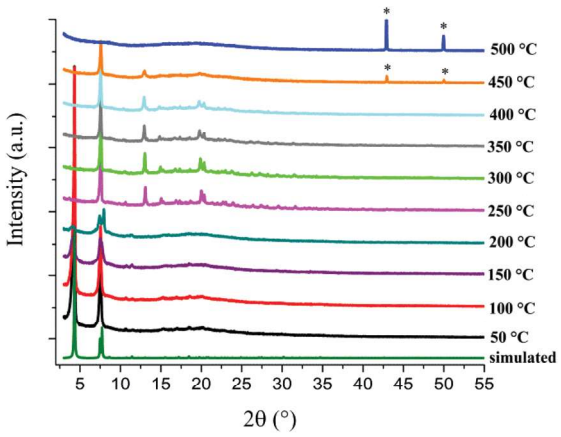

Fig. 5 VTXRPD plots of **Cu(I)[CFA-4]** in the range of 50–500 °C. The dark green XRPD pattern is simulated based on single crystal X-ray data. *peaks belong to Cu phase (PDF no. 4-836).

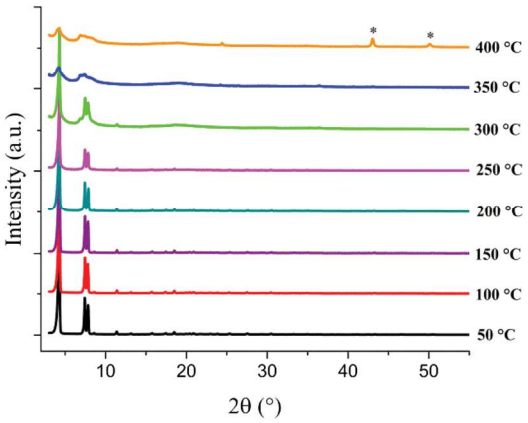

Fig. 6 VTXRPD plots of **K[CFA-4]** in the range of 50–400 °C. *Peaks belong to Cu phase (PDF no. 4-836).

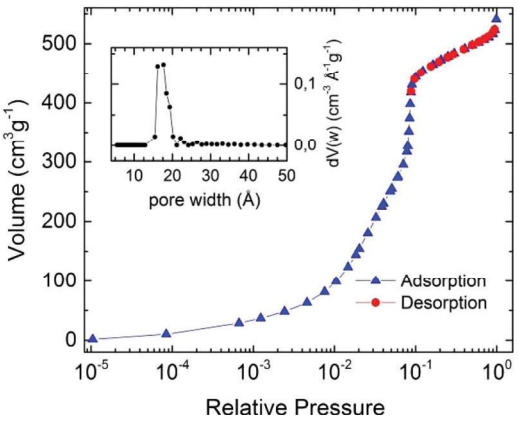

Fig. 7 Argon adsorption (blue) and desorption (red) isotherms of **K[CFA-4]** at 87 K. Inset: Pore size distribution calculated from these isotherms.

2224.4 Å^3 (DICVOL, M_{20} = 151, F_{20} = 30.7 (0.0059, 111)) and a = 16.739 Å, b = 16.029 Å, c = 8.344 Å, V = 2238.8 Å^3 (TREOR, M_{20} = 12, F_{20} = 23 (0.012035, 73)). Above 400 °C the decomposition of the compound is observed and Cu (PDF no. 4-836) appears as a new crystalline phase.

Partial exchange of the coordinated DMF molecules in **Cu(I)[CFA-4]** by acetonitrile, leads to a sample crystalline up to 400 °C. The VTXRPD of this sample with the composition **Cu (I)[Cu$_5$(tfpb)$_3$]·2.5CH$_3$CN·0.5DMF** (as determined from the TGA data) are plotted in ESI (Fig. S14†).

Variable temperature X-ray powder diffraction studies of **K[CFA-4]** (Fig. 6) are in good agreement with the results from the TGA measurement. The framework is stable up to at least 250 °C. Above this temperature, the decomposition of the compound is observed and Cu (PDF no. 4-836) appears as a new crystalline phase at 400 °C in the VTXRPD.

Gas sorption measurements

Argon gas sorption measurements on **Cu(I)[CFA-4]** and **K[CFA-4]** at 87 K confirm permanent porosity of both frameworks. Prior to the measurement, the sample of **Cu(I)[CFA-4]** was washed with DMF and methanol (**K[CFA-4]** with MeOH) and heated at 100 °C in high vacuum for 20 hours to remove occluded solvent molecules. The resulting argon adsorption/desorption isotherms of both samples follow type I behavior, which is characteristic for microporous solids. The maximum uptake achieved at 87 K and p/p_0 = 0.99 is 459 cm^{-3} g^{-1} for **Cu(I)[CFA-4]** (ESI, Fig. S21†) and 541 cm^{-3} g^{-1} for **K[CFA-4]** (Fig. 7), corresponding to a total pore volume of 0.58 and 0.69 cm^3 g^{-1}, respectively (Fig. 7).

The micropore volume of **K[CFA-4]** determined at p/p_0 = 0.2 is 0.60 cm^3 g^{-1} which corresponds well to the value calculated from the crystal structure data (0.64 cm^3 g^{-1}). The BET surface area determined in the range p/p_0 = 0.1–0.16 is 1431 m^2 g^{-1}. To evaluate the pore size distribution of the **CFA-4** framework, the argon sorption isotherms sampled for **K[CFA-4]** at 87 K were analysed using non-local density functional theory (NLDFT)[28] implementing a carbon equilibrium transition kernel for argon adsorption based on a slit-pore model.[29] The distribution calculated by fitting the adsorption data reveals micropores with a diameter in the range of 13–20 Å with a maximum at 17 Å (Fig. 7, inset) which is in good agreement with the crystal structure data.

Cu(I)[CFA-4], due to the presence of coordinated DMF molecules, shows a slightly lower BET surface area of 1324 m^2 g^{-1} (determined in the range p/p_0 = 0.09–0.12). The high-temperature phase of **Cu(I)[CFA-4]** (obtained after heating the sample at 350 °C in vacuum) exhibits permanent porosity as well, but the specific surface area decreases to 600 m^2 g^{-1} (for the isotherm see ESI, Fig. S22†).

The isosteric heat of CO adsorption for **Cu(I)[CFA-4]** determined from adsorption isotherms measured in the temperature range 183–203 K (see ESI, Fig. S24†) reaches a rather high value of 52 kJ mol^{-1} at low loading (<0.05 mmol g^{-1}) and decreases to typical physisorption values of <15 kJ mol^{-1} at >0.6 mmol g^{-1} loading (Fig. 8, green curve). Such behavior hints at a weak binding of carbon monoxide to the interchannel Cu(I) cations of **Cu(I)[CFA-4]**. The copper centres of the

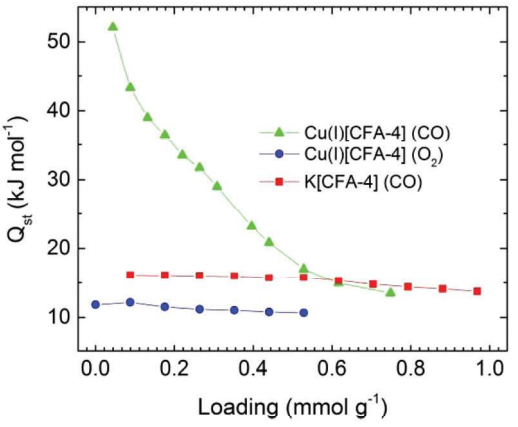

Fig. 8 Isosteric heats of CO (green) and O_2 (blue) adsorption in **Cu(I)[CFA-4]** and CO adsorption in **K[CFA-4]** (red).

SBU of **M[CFA-4]** are well-shielded by the CF_3-groups and not freely accessible to bind small molecules. The amount of active Cu(I)-sites roughly estimated from the dependence of the isosteric heat of CO adsorption on loading (approx. 0.5 mmol g^{-1}) corresponds well to the calculated amount of Cu(I) cations in the channels (0.51 mmol g^{-1}). Binding of CO at the interchannel Cu(I) cations is also confirmed by CO sorption measurements on **K[CFA-4]** (see ESI, Fig. S25†), revealing an isosteric heat of adsorption of only 14–16 kJ mol^{-1} (Fig. 8, red curve). Oxygen adsorption isotherms for **Cu(I)[CFA-4]** (see ESI, Fig. S23†) reveal nearly constant physisorption heat of 11–12 kJ mol^{-1} (Fig. 8, blue curve) and thus show that interchannel Cu(I) cations do not bind O_2 molecules.

In addition, the adsorption of CO in **Cu(I)[CFA-4]** was studied by diffuse reflectance Fourier-transform IR spectroscopy (DRIFT) (see Fig. 9). First, the sample was heated up to 160 °C under nitrogen flow. After cooling down to room temperature, an FT-IR spectrum of the activated **Cu(I)[CFA-4]** was recorded under nitrogen. Then, the gas flow was switched to CO and another spectrum was recorded. The bands at 2171 cm^{-1} and 2132 cm^{-1} at room temperature (black line) belong to free CO molecules in the gas phase. The temperature was gradually decreased in 20 °C steps down to −90 °C. At this temperature, the gas flow was changed to nitrogen again, followed by the stepwise heating up to 50 °C. Below 0 °C, new bands at 2046 cm^{-1} (with a shoulder at 2055 cm^{-1}) and 2157 cm^{-1} (assigned in Fig. 9 as 1 and 1a, respectively) were detected. Moreover, the intensity of the band at 2132 cm^{-1} as well as for the both new bands 1 and 1a increase upon cooling process. These bands result from CO molecules bound to the interchannel Cu(I) ions, as already shown by enhanced isosteric heat of CO adsorption (Fig. 8). At −60 °C a new band at 2127 cm^{-1} (2) appears, which splits into two bands at −90 °C with wavenumbers of 2108 cm^{-1} (2a) and 2144 cm^{-1} (2b), while the band at 2132 cm^{-1} disappears. We assume that a second CO molecule binds to the same Cu(I) center at low temperatures leading to the observed band splitting and vanishing of the band at 2132 cm^{-1}. All these low-temperature bands (2, 2a and 2b) disappear rapidly after switching from a CO to N_2-atmosphere while the bands 1 and 1a remain up to 0 °C. This observation confirms our assumption for a weak binding of the second CO molecule.

All these recorded bands correspond to the stretch mode of the CO molecules coordinatively bound to Cu^{I}-ions and are in good agreement with literature data of Cu(I)–pyrazolate complexes (ν_{CO} = 2137 cm^{-1} for [Cu{HB(3,5-$(CF_3)_2$$pz_3$}(CO)],[30] 2102 cm^{-1} for [Cu{HB(3-$C_3F_7$$pz_3$)}(CO)][31] and 2056 cm^{-1} for [Cu{HB(3,5-i$Pr_2$$pz)_3$}(CO)]).[32]

Photoluminescence and UV-Vis spectroscopy

Solid-state photoluminescence properties of **1**, **K[CFA-4]** and **Cu(I)[CFA-4]** were studied at room temperature. The ligand H_2-tfpb (**1**) exhibits a broad emission peak under excitation at 248 nm (Fig. 10). **1** shows maximum emission at around 340–350 nm and a smaller emission shoulder at 312 nm. Excitation of **1** with an emission wavelength of 340 nm leads to a broad excitation spectrum with a main maximum at 245 nm and a side maximum at 285 nm. Excitation at higher wavelength (290 nm) results in one emission maximum at 350–355 nm whereas the shoulder at 312 nm disappears (see ESI Fig. S33†). The excitation of **1** is probably attributed to the $\pi \rightarrow \pi^*$ transition of the aromatic system. Due to the presence of CF_3-groups, the ligand is twisted and has no entirely delocalised flat π-system, resulting in two possible $\pi \rightarrow \pi^*$ transitions (corresponding to phenyl- and pyrazolate-rings). With higher energy (248 nm), excitation of both transitions is possible, whereas at smaller energy (290 nm) only one process can be excited. CF_3-groups at the pyrazolate-units have a strong electron-withdrawing effect. As a consequence, a higher photon energy is necessary for the excitation process. The excitation spectrum (λ_{em} = 312 nm) shows only one maximum at 245 nm, whereas a maximum at 290 nm disappears (see ESI Fig. S32†). Based on these observations, we presume that the emission at 312 nm results from the CF_3-substituted pyrazolate rings of the ligand.

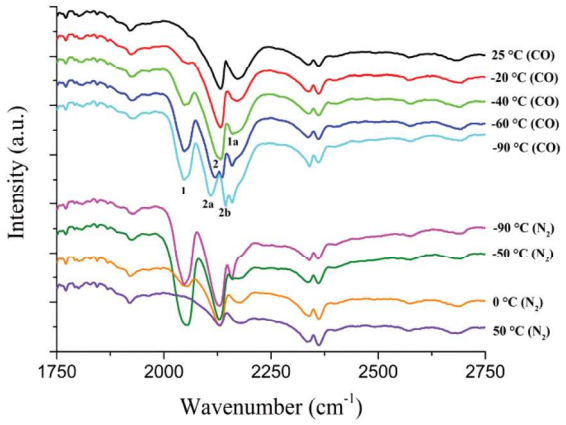

Fig. 9 *In situ* DRIFT spectra of **Cu(I)[CFA-4]** upon cooling from room temperature to −90 °C under CO atmosphere and subsequent heating from −90 °C to 50 °C under N_2 atmosphere.

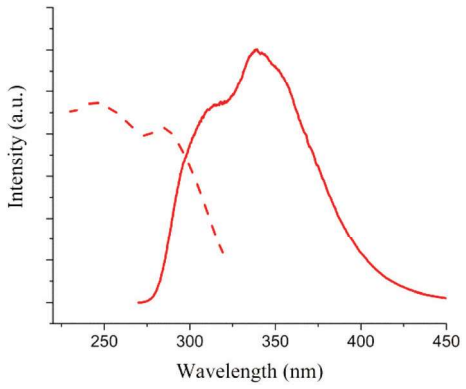

Fig. 10 Solid-state photoluminescence spectra of **1** at room temperature. Dashed line: excitation spectrum (λ_{em} = 340 nm); continuous line: emission spectrum (λ_{ex} = 248 nm).

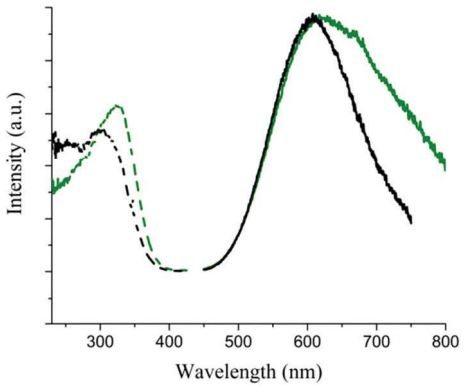

Fig. 11 Solid-state photoluminescence spectra of **K[CFA-4]** (green) and **Cu(I)[CFA-4]** (black) at room temperature. Dashed line: excitation spectrum (λ_{em} = 620 nm for **K[CFA-4]** and 610 nm for **Cu(I)[CFA-4]**); continuous line: emission spectrum (λ_{ex} = 325 nm for **K[CFA-4]** and 305 nm for **Cu(I)[CFA-4]**).

Fig. 11 shows photoluminescence spectra for **K[CFA-4]** (green line) and **Cu(I)[CFA-4]** (black line). A broad emission can be observed for both frameworks in the visible region between 500 nm and 750 nm under excitation with the UV light (325 nm for **K[CFA-4]** and 305 nm for **Cu(I)[CFA-4]**), while the emission of the ligand disappears. Compared to **Cu(I)[CFA-4]**, the resulting emission band of **K[CFA-4]** is bathochromically shifted to lower energies. This shift indicates a stronger Cu···Cu interaction in **Cu(I)[CFA-4]** due to the presence of free Cu(I)-cations in the pores instead of potassium cations. To achieve low-energy emission, the Cu–Cu distance normally must be less than or close to twice the van der Waals radius of Cu^{I} (1.4 Å). The closest Cu–Cu distance in **K[CFA-4]** is 3.154 Å and should be too large to influence the luminescence properties by intramolecular Cu···Cu interactions. We presume that the emission here is probably related to a metal-to-ligand charge transfer. Upon irradiation with the UV light Cu(I) pyrazolates undergo a metal-to-ligand charge transfer resulting in a charge-separated excited singlet state. This state can either decay to the ground state by the emission of slightly red-shifted photons, or undergo a spin conversion into an excited triplet state, which shows a slow decay (luminescence) to the ground state.[33] The latter transition might be influenced by weak Cu···Cu interactions that typically occur in Cu(I) complexes and coordination polymers comprising bridging pyrazolate moieties.

Moreover the influence of different solvents on the fluorescence behaviour of **Cu(I)[CFA-4]** was investigated (see ESI Fig. S34†). The intensity of the emission maximum strongly depends on the adsorbed solvent molecules. A significant fluorescence quenching can be observed upon addition of nitroaromatic compounds such as nitrobenzene or dinitrophenol (solution in methanol). This observation could qualify **M[CFA-4]** interesting as a potential material for selective sensing of nitroaromatics.

To demonstrate the sensitivity of **M[CFA-4]** towards nitroaromatic compounds, it was exposed to a vapour of nitrobenzene for various time periods at room temperature. During the experiment, fluorescence was strongly reduced within a few minutes (Fig. 12). The emission could be regenerated after placing the sample into high vacuum for several hours or simply by washing it with ethanol, what makes this "turn-on" and "turn-off" fluorescence to a fully reversible process.

In literature, several examples of MOFs with such selective sensing behaviour towards highly electron withdrawing nitroaromatic compounds have already been reported.[34] The observed fluorescence quenching is attributed to a photo-induced electron transfer from the excited MOF to the electron deficient analytes adsorbed on the MOF surface.

To prove the reactivity of **K[CFA-4]** and **Cu(I)[CFA-4]** towards molecular oxygen, the samples were investigated with UV-vis spectroscopy (see Fig. 13). Freshly prepared **K[CFA-4]** (red curve) and **Cu(I)[CFA-4]** (black curve) show one strong absorption peak at 291 nm in the solid-state UV-vis spectrum. Oxidation of **Cu(I)[CFA-4]** in air is a slow process entailing a color change to dark green. The UV-vis spectrum of the oxi-

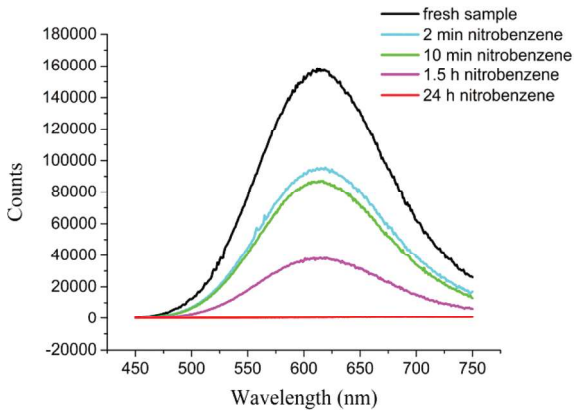

Fig. 12 Solid-state photoluminescence spectra of **Cu(I)[CFA-4]** exposed to a nitrobenzene vapour at room temperature for various time periods (excitation wavelength 320 nm).

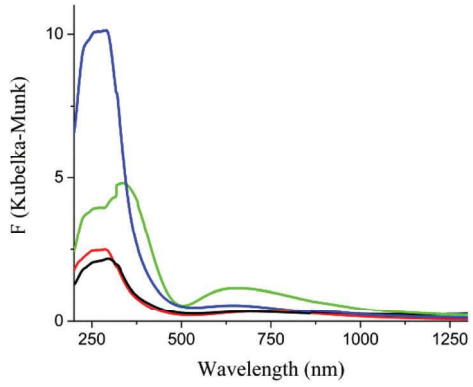

Fig. 13 UV-vis spectra of **M[CFA-4]** at room temperature. Red line: **K[CFA-4]** freshly prepared; black line: **Cu(I)[CFA-4]** freshly prepared; green line: **Cu[CFA-4]** oxidised; blue line: **Cu(I)[CFA-4]** reduced.

dised **Cu[CFA-4]** (green curve) exhibits a peak shift at small wavelength and one additional peak with a maximum at 656 nm, which encompasses the Cu^{II} d–d transitions.

Furthermore, the oxidised **Cu[CFA-4]** can be reduced to a Cu(I) compound upon heating in DMF at 120 °C for 4 hours (blue curve). After four weeks in air, **K[CFA-4]** shows a UV-vis spectrum which is similar to the fresh sample. This leads to the assumption that the SBU of **M[CFA-4]** is stable against oxidation, as the copper centres are well-shielded by the CF_3-groups. This stability against oxidation is another benefit for potential application in photonic research.

The XRPD patterns of the oxidised and reduced samples (see ESI Fig. S15†) are similar to the freshly prepared, indicating that the structure remains stable during the oxidation/reduction sequence. Unfortunately, a single crystal analysis of oxidised **Cu[CFA-4]** was not successful due to very weak scattering of the crystals.

Conclusions

The work reported here describes the synthesis and characterisation of a novel metal–organic framework **M[CFA-4]** assembled from pentanuclear copper(I) secondary building units $\{Cu^{I}_{5}(pz)_6\}^-$ and fluorinated bifunctional ligands. To the best of our knowledge, **M[CFA-4]** represents the first example of a MOF in which a pentanuclear copper(I)-containing SBU was found and structurally characterized. This framework crystallizes in the hexagonal crystal system within the chiral space group $P6_322$ and features channels with a narrowest diameter of 14.3 Å. Due to a negative charge of the lattice, the channels of the as-synthesized framework are occupied by Cu^+ ions, which can be readily exchanged with K^+, Cs^+ or Ca^{2+}. After removal of the solvent, the Cu^+ ions are reactive and can bind CO with isosteric heat of adsorption of up to 52 kJ mol^{-1}. **M[CFA-4]** remains porous after solvent removal and exhibits the BET surface area of 1591 m^2 g^{-1} (**K[CFA-4]**).

1 and **M[CFA-4]** show interesting fluorescent properties. **M[CFA-4]** shows high porosity, large open pores, a good stability towards many solvents and interesting selective and sensitive fluorescence behaviour towards nitroaromatics. This property, combined with the possibility to exchange metal ions in the channels, suggests **M[CFA-4]** as a promising framework for the development of new photoluminescent materials and for applications in sensor technology.

Furthermore, MOFs with fluorinated ligands seem to have high photostability. Therefore they could be very interesting for applications as photocatalysts, for redox reactions or for solar fuel production.[35]

Experimental section

Materials and general methods

All starting materials were of analytical grade and used as obtained from commercial sources without further purification. Thermogravimetric analysis (TGA) was performed with a TGA Q500 analyser in the temperature range of 25–800 °C in a flowing nitrogen gas at a heating rate of 10 K min^{-1}. NMR spectra were recorded on a Varian mercury plus 400 high resolution system; data given in ppm; spectra referenced to the residual solvent peak. Fourier transform infrared (FTIR) spectra were recorded with an ATR unit in the range of 4000–400 cm^{-1} on a Bruker Equinox 55 FT-IR spectrometer. Diffuse reflectance infrared Fourier-transformed (DRIFT) spectra were recorded with the same instrument equipped with a Harrick Praying Mantis I21012 reaction chamber. Energy-dispersive X-ray spectroscopy (EDX) was performed with a Philips XL-30 scanning electron microscope. Ambient temperature X-ray powder diffraction (XRPD) patterns were recorded on a Seifert XRD 3003 TT diffractometer equipped with a Meteor1D detector operated at 40 kV, 40 mA, Cu Kα (λ = 1.54178 Å) with a scan speed of 1 s per step and a step size of 0.02° in 2θ. Variable temperature X-ray powder diffraction (VTXRPD) measurements were collected in the 2θ range of 3–60° with 0.02° steps with a Bruker D8 Advance diffractometer equipped with a Lynxeye linear position-sensitive detector, a MRI TCPU1 oven, in linear transmission geometry. The sample was loaded into a capillary (Hilgenberg) made from special glass no. 10, 0.5 mm diameter and 0.01 mm wall thickness. The patterns were recorded in a temperature range from 30 to 500 °C, in the 3–60° 2θ range, with one step per 1 s, and an angular step width of 0.02° in 2θ. Temperature program between measurements: heating rate (0.5 °C s^{-1}), then 10 min isothermal. Argon gas sorption isotherms at 77 K were measured with a Quantachrome Autosorb-I ASI-CP-8 instrument. Ar (87 K), CO and O_2 sorption isotherms were measured with a BELSORP-max instrument combined with a BELCryo system. Adsorbed gas amounts are given in cm^3 g^{-1} [STP], where STP = 101.3 kPa and 273.15 K. High-resolution mass spectra were recorded with a Q-Tof Ultima Mass spectrometer (Micromass) equipped with an ESI source. The elemental composition of molecular ions was verified by comparison between experimental and theoretical mass values and isotopic distributions. Luminescence spectra were acquired using a spectrofluorimeter (FS920, Edinburgh Instruments) equipped with a TMS300 monochromator, an S900 single photon photomultiplier, and a Xe 900 450 W xenon arc lamp at r. t. The excitation and emission spectra were corrected for the wavelength-dependent lamp intensity and detector response, respectively.

Synthesis of H_2-tfpb (1)

4-Iodo-3,5-bis(trifluoromethyl)-1*H*-pyrazole[22] was synthesized from 3,5-bis(trifluoromethyl)-1*H*-pyrazole *via* a modified iodination procedure, similarly to the literature-described procedure for other pyrazole derivatives.[36]

3,5-Bis(trifluoromethyl)-1*H*-pyrazole (4.00 g; 19.61 mmol), iodine (2.97 g; 11.76 mmol) and cerium(IV) ammonium nitrate (5.37 g; 9.80 mmol) were dissolved in acetonitrile (160 mL). After stirring for 30 minutes at room temperature, the brown mixture was refluxed for 34 h, cooled to room temperature and the solvent was removed with a rotary evaporator. The residue

was dissolved in ethyl acetate (400 mL) and washed with ice-cold sodium hydrogen sulphite solution (5%; 400 mL). The aqueous phase was once again extracted with ethyl acetate (200 mL), before the combined organic phase was washed with brine (200 mL). The solvent was removed under reduced pressure and the residue was dried under vacuum affording pure 4-iodo-3,5-bis(trifluoromethyl)-1*H*-pyrazole (5 g; 78%). Analytical data correspond to the previously described.[22]

1,4-Bis(4,4,5,5-tetramethyl-1,3,2-dioxaborolan-2-yl)benzene (1.19 g; 3.60 mmol) and 4-iodo-3,5-bis(trifluoromethyl)-1*H*-pyrazole (2.85 g; 8.64 mmol) were dissolved in 120 mL of 1,2-dimethoxyethane (DME). A solution of K_2CO_3 (1.99 g; 14.4 mmol) in water (85 mL) was added. The reaction mixture was degassed in vacuum by a freezing method and flooded with argon. Tetrakis(triphenylphosphine)palladium(0) (416 mg; 0.36 mmol) was added and the reaction vessel was degassed and flooded again. After reflux for 48 h and cooling to room temperature, DME was removed with a rotary evaporator. Water (20 mL) and brine (20 mL) were added and extracted with EtOAc (3 × 100 mL). The combined organic phase was washed with brine (150 mL) and dried over $MgSO_4$. After removal of the solvent under reduced pressure, the solid was dried under vacuum overnight. Column chromatography on silica gel with a $CHCl_3$: EtOAc (15 : 1) mixture led to the raw product. Analytically pure 1,4-bis(3,5-bis(trifluoromethyl)-1*H*-pyrazole-4-yl)benzene was obtained after recrystallization of the raw product from methanol. Single crystals of **1** for X-ray diffraction experiment were obtained by slow evaporation of the methanolic solution.

Yield: 660 mg (39%). ^{1}H-NMR (400 MHz, DMSO-d_6, δ (ppm)): 7.40 (s, 4H, CH), 15.39 (s, 2H, NH). ^{1}H-NMR (400 MHz, acetone-d_6, δ (ppm)): 7.55 (s, 4H, CH). ^{19}F-NMR (400 MHz, DMSO-d_6, δ (ppm)): −57.65 (s, 12F, CF_3). ^{19}F-NMR (400 MHz, acetone-d_6, δ (ppm)): −59.68 (s, 12F, CF_3). ^{13}C-NMR (400 MHz, acetone-d_6, δ (ppm)): 130.6 (s), 129.4 (s), 121.6 (s), 121.3 (q, J = 267 Hz). IR (ν(cm^{-1})): 2915; 1540; 1491; 1435; 1304; 1231; 1197; 1136; 981; 847; 767; 655; 552; 488; 432. ESI + TOF HRMS m/z 483.0475 ([M + H]$^+$, calculated for $C_{16}H_6F_{12}N_4$ + H^+: 483.0474). The NMR-, IR- and mass-spectra of **1** are shown in the ESI (S4–10, S17 and Table S2†).

Synthesis of Cu(I)[Cu_5(tfpb)$_3$]·4.75DMF

Solvothermal method. A mixture of copper nitrate trihydrate (10 mg; 0.04 mmol) and H_2-tfpb (10 mg, 0.02 mmol) was dissolved in 3 mL DMF (alternative: 3 mL MeOH and 0.0 5 ml 2,6-lutidine) and the solution was placed in a glass tube (10 mL). The tube was closed and heated at 120 °C for 3 days and then cooled to room temperature. The precipitate was filtered and washed with DMF and MeOH and dried at 100 °C under vacuum. This synthesis can be similarly performed at larger quantities (upscale factor: 20).

Yield: 16 mg (43%). IR (ν(cm^{-1})): 2359; 1665; 1498; 1350; 1314; 1218; 1134; 1028; 995; 854; 739; 722; 671; 622; 553; 432. The IR-spectra of **Cu(I)[CFA-4]** are shown in ESI (S9–11†).

Microwave synthesis. A mixture of copper nitrate trihydrate (10 mg; 0.04 mmol) and H_2-tfpb (10 mg, 0.02 mmol) was dissolved in 3 mL DMF (alternative: 3 mL MeOH and 0.05 ml 2,6-lutidine) and the solution was placed in a Pyrex sample tube (10 mL). The tube was closed with a cap and placed in a microwave synthesizer (CEM, Discover S). The resulting mixture was heated to 150 °C at 300 W for 20 min and cooled to room temperature. The precipitate was filtered and washed with DMF and MeOH and dried at 100 °C under vacuum.

Yield: 9 mg (25%). This material exhibited the same analytical results for IR- and XRD-measurements as the ones obtained by the solvothermal method.

Synthesis of Cu(I)[Cu_5(tfpb)$_3$]·2.5CH_3CN·0.5DMF

Cu(I)[CFA-4]·2.5CH_3CN·0.5DMF was synthesised by soxhlet extraction of **Cu(I)[CFA-4]** in acetonitrile (3 × 2 h) under argon atmosphere. Finally the sample was dried under argon.

General synthesis procedure for M[Cu_5(tfpb)$_3$] (M = K, Cs, Ca (0.5))

Cu(I)[CFA-4] (55 mg; 0.03 mmol) was stirred at room temperature for 2 h in a solution of the corresponding metal nitrate (0.6 mmol for K^+ and Cs^+, 0.3 mmol for Ca^{2+}) in DMF (2.5 mL) and H_2O (0.5 mL). The precipitate was filtered, washed with water (2 × 3 mL), DMF (2 × 3 mL) and MeOH (2 × 3 mL). This exchange procedure was repeated three times. The Cu/M molar ratio of the product was determined by energy dispersive X-Ray spectroscopy.

Single-crystal X-ray crystallography

X-ray data for the single crystal structure of **1**·2MeOH were collected on a Bruker D8 Venture diffractometer. Intensity measurements were performed using monochromated (doubly curved silicon crystal) MoKα radiation (0.71073 Å) from a sealed microfocus tube. Generator settings were 50 kV, 1 mA. Data collection temperature was −173 °C. APEX2 software was used for preliminary determination of the unit cell.[37] Determination of integrated intensities and unit cell refinement were performed using SAINT.[38] The structure was solved and refined using the Bruker SHELXTL Software Package.[39] Selected crystal data and details of structure refinement for **1·2MeOH** are provided in Table 1.

X-ray data for the single crystal structure of **Cu(I)[CFA-4]** were collected at 295 K using synchrotron radiation with energy of 14 keV (λ = 0.88561 Å) on BESSY MX BL14.2 beamline of Helmholtz Zentrum Berlin für Materialien und Energie.[40] The single crystal was transferred to a glass capillary with some amount of solvent. The φ-scans with oscillation range of 1° were used for data collection. The data were integrated and scaled with the XDS software package.[41] The structure was solved using direct methods with the help of SHELXS-97 and refined by full-matrix least squares techniques using SHELXL Version 2016/1.[42] **Cu(I)[CFA-4]** was refined as a racemic twin, with the inversion matrix TWIN −100 0−10 00−1 and the BASF coefficient 0.49. Non-hydrogen atoms were refined with anisotropic temperature parameters. The hydrogen atoms were positioned geometrically and refined using a riding model. The positions of the disordered solvent molecules and Cu(I)-ions

Table 1 Crystal data and structure refinement of **1**·2MeOH and **Cu(I)[CFA-4]**

Compound	**1**·2MeOH	**Cu(I)[CFA-4]**·4.75DMF
Empirical formula	$C_{18}H_{14}F_{12}N_4O_2$	$C_{62.25}H_{45.25}Cu_6F_{36}N_{16.75}O_{4.75}$
Formula	$C_{16}H_6F_{12}N_4$, 2 (CH_3OH)	$Cu(I)[Cu_5(C_{16}H_4F_{12}N_4)_3]$·4.75 ($C_3H_7NO$)
M_r/g mol^{-1}	546.33	2169.14
T/K	100(2)	295(2)
Wavelength/Å	0.71073	0.88561
Crystal system	Monoclinic	Hexagonal
Space group	$C2/m$ (no. 12)	$P6_322$ (no. 182)
a/Å	8.8990(5)	23.630(5)
b/Å	14.7907(7)	23.630(5)
c/Å	8.9987(8)	41.390(5)
α/°	90	90
β/°	111.494(2)	90
γ/°	90	120
V/Å^3	1102.06(13)	20 015(6)
Z	2	6
D_c/g cm^{-3}	1.646	1.080
μ/mm^{-1}	0.177	1.856
F(000)	548	6432
θ Range/°	2.43 to 25.08	2.23 to 36.16
Refls. collected	12 273	81 573
Refls. unique	1026	15 739
R(int)	0.0491	0.0833
GooF	0.945	0.983
Flack parameter	—	0.490(13)
R_1 ($I > 2\sigma(I)$][a]	0.0286	0.0506
wR_2 (all data)[b]	0.0720	0.1656
Largest diff. peak and hole/Å^{-3}	0.334 and −0.221	0.549 and −0.515

[a] $R_1 = \sum||F_o| - |F_c||/\sum|F_o|$. [b] $wR_2 = \sum[w(F_o^2 - F_c^2)2]/\sum[w(F_o^2)2]^{1/2}$.

were impossible to resolve and to refine from the electron density distribution. The SQUEEZE procedure implemented in the program PLATON[24] was used and an electron count of 1312 per unit cell (rest of the electron density) was calculated. This value corresponds to 6 Cu(I)-ions and 28.5 DMF molecules in the unit cell of **Cu(I)[CFA-4]**. Thus, the composition of the framework was determined as $[Cu_5(tfpb)_3]^-$ (Cu^+)·4.75DMF. Complete crystallographic data for the structures **1**·2MeOH and **Cu(I)[Cu$_5$(tfpb)$_3$]**·4.75DMF reported in this paper have been deposited in the CIF format with the Cambridge Crystallographic Data Center, 12 Union Road, Cambridge CB21EZ, UK as supplementary publication no. CCDC 1532837 and 1532600, respectively.

Acknowledgements

Financial support by the DFG (Priority Program SPP 1362 "Porous Metal–Organic Frameworks") is gratefully acknowledged. We thank HZB for the allocation of synchrotron radiation beamtime.

Notes and references

1 (*a*) M. P. Suh, H. J. Park, T. K. Prasad and D.-W. Lim, *Chem. Rev.*, 2012, **112**, 782–835; (*b*) I. Senkovska and S. Kaskel, *Microporous Mesoporous Mater.*, 2008, **112**(1–3), 108–115; (*c*) L. J. Murray, M. Dinca and J. R. Long, *Chem. Soc. Rev.*, 2009, **38**, 1294–1314; (*d*) H. Furukawa, K. E. Cordova, M. O'Keeffe and O. M. Yaghi, *Science*, 2013, **341**, 974.

2 (*a*) J. An, S. J. Geib and N. L. Rosi, *J. Am. Chem. Soc.*, 2009, **131**, 8376–8377; (*b*) N. P. E. Barry, O. Zava, P. J. Dyson and B. Therrien, *Chem. – Eur. J.*, 2011, **17**, 9669–9677; (*c*) P. Horcajada, C. Serre, G. Maurin, N. A. Ramsahye, F. Balas, M. Vallat- Regí, M. Sebban, F. Taulelle and G. Férey, *J. Am. Chem. Soc.*, 2008, **130**, 6774–6780; (*d*) E. Quartapelle Procopio, S. Rojas, N. M. Padial, S. Galli, N. Masciocchi, F. Linares, D. Miguel, J. E. Oltra, J. A. R. Navarro and E. Barea, *Chem. Commun.*, 2011, **47**, 11751–11753.

3 (*a*) L. E. Kreno, K. Leong, O. K. Farha, M. Allendorf, R. P. Van Duyne and J. T. Hupp, *Chem. Rev.*, 2012, **112**, 1105–1125; (*b*) O. Shekhah, J. Liu, R. A. Fischer and Ch. Wöll, *Chem. Soc. Rev.*, 2011, **40**, 1081–1106; (*c*) S. T. Meek, J. A. Greathouse and M. D. Allendorf, *Adv. Mater.*, 2011, **23**, 249–267.

4 (*a*) J. Teufel, H. Oh, M. Hirscher, M. Wahiduzzaman, L. Zhechkov, A. Kuc, T. Heine, D. Denysenko and D. Volkmer, *Adv. Mater.*, 2013, **25**, 635–639; (*b*) H. Oh, I. Savchenko, A. Mavrandonakis, T. Heine and M. Hirscher, *ACS Nano*, 2014, **8**, 761–770; (*c*) E. Quartapelle Procopio, F. Linares, C. Montoro, V. Colombo, A. Maspero, E. Barea and J. A. R. Navarro, *Angew. Chem., Int. Ed.*, 2010, **49**, 7308–7311; (*d*) P. D. C. Dietzel, V. Besikiotis and R. Blom, *J. Mater. Chem.*, 2009, **19**, 7362–7370.

5 (*a*) D. Farrusseng, S. Aguado and C. Pinel, *Angew. Chem., Int. Ed.*, 2009, **121**, 7638–7649; (*b*) J. Liu, L. Chen, H. Cui, J. Zhang, L. Zhang and C.-Y. Su, *Chem. Soc. Rev.*, 2014, **43**, 6011–6061; (*c*) M. Tonigold, Y. Lu, A. Mavrandonakis, A. Puls, R. Staudt, J. Möllmer, J. Sauer and D. Volkmer, *Chem. – Eur. J.*, 2011, **17**, 8671–8695.

6 (*a*) C. Yang, X. Wang and M. A. Omary, *J. Am. Chem. Soc.*, 2007, **129**, 15454–15455; (*b*) C. Yang, X. Wang and M. A. Omary, *Angew. Chem., Int. Ed.*, 2009, **48**, 2500–2505.

7 (*a*) *Handbook of Fluorous Chemistry*, ed. J. A. Gladysz, D. P. Curran and I. T. Horváth, Wiley-VCH, Weinheim, Germany, 2004; (*b*) I. T. Horváth and J. Rabai, *Science*, 1994, **266**, 72–75; (*c*) P. T. Nyffeler, S. G. Durón, M. D. Burkart, S. P. Vincent and C.-H. Wong, *Angew. Chem., Int. Ed.*, 2005, **44**, 192–212.

8 M. Pagliaro and R. Ciriminna, *J. Mater. Chem.*, 2005, **15**, 4981–4991.

9 T.-H. Chen, I. Popov, W. Kaveevivitchai, Y.-C. Chuang, Y.-S. Chen, A. J. Jacobson and O. Š. Miljanić, *Angew. Chem., Int. Ed.*, 2015, **127**, 14108–14112.

10 D.-S. Zhang, Z. Chang, Y.-F. Li, Z.-Y. Jiang, Z.-H. Xuan, Y.-H. Zhang, J.-R. Li, Q. Chen, T.-L. Hu and X.-H. Bu, *Sci. Rep.*, 2013, **3**, 3312.

11 C. G. Piscopo, F. Trapani, A. Polyzoidis, M. Schwarzer, A. Pace and S. Loebbecke, *New J. Chem.*, 2016, **40**, 8220–8224.

12 M. C. Das, S. C. Xiang, Z. J. Zhang and B. L. Chen, *Angew. Chem., Int. Ed.*, 2011, **50**, 10510–10520.

13 (*a*) Z. Hu, B. J. Deibert and J. Li, *Chem. Soc. Rev.*, 2014, **43**, 5815–5840; (*b*) Y. Li, S. S. Zhang and D. T. Song, *Angew. Chem., Int. Ed.*, 2013, **52**, 710–713; (*c*) D. Liu, K. Lu, C. Poon and W. B. Lin, *Inorg. Chem.*, 2014, **53**, 1916–1924.
14 S. E. Miller, M. H. Teplensky, P. Z. Moghadam and D. Fairen-Jimenez, *Interface Focus*, 2016, **6**, 20160027.
15 (*a*) A. Barba-Bon, A. M. Costero, S. Gil, M. Parra, J. Soto, R. Martínez- Máñezac and F. Sancenón, *Chem. Commun.*, 2012, **48**, 3000–3002; (*b*) A. M. Costero, J. V. Colomer, S. Gil and M. Parra, *Eur. J. Org. Chem.*, 2009, 3673–3677.
16 J. An, C. M. Shade, D. A. Chengelis-Czegan, S. Petoud and N. L. Rosi, *J. Am. Chem. Soc.*, 2011, **133**, 1220–1223.
17 B. Chen, L. Wang, Y. Xiao, F. R. Fronczek, M. Xue, Y. Cui and G. Qian, *Angew. Chem., Int. Ed.*, 2009, **48**, 500–503.
18 J. A. Hurd, R. Vaidhyanathan, V. Thangadurai, C. I. Ratcliffe, I. L. Moudrakovski and G. K. H. Shimizu, *Nat. Chem.*, 2009, **1**, 705–710.
19 P. Schmieder, D. Denysenko, M. Grzywa, O. Magdysyuk and D. Volkmer, *Dalton Trans.*, 2016, **45**, 13853–13862.
20 M. Grzywa, D. Denysenko, A. Schaller, A. Kalytta-Mewes and D. Volkmer, *CrystEngComm*, 2016, **18**, 7883–7893.
21 D. Denysenko, M. Grzywa, J. Jelic, K. Reuter and D. Volkmer, *Angew. Chem., Int. Ed.*, 2014, **53**, 5832–5836.
22 A. Maspero, G. B. Giovenezana, D. Monticelli, S. Tagliapietra, G. Palmisano and A. Penoni, *J. Fluorine Chem.*, 2012, **139**, 53–57.
23 M. Kleinwächter, L. Vendier, C. Dinoi and M. Etienne, *Dalton Trans.*, 2013, **42**, 10102.
24 A. L. Spek, *Acta Crystallogr., Sect. C: Cryst. Struct. Commun.*, 2015, **71**, 9–18.
25 *Quantachrome Autosorb, Version 1.56*, 2009.
26 V. A. Blatov, IUCr CompComm Newsletter, 2006, **7**, 4–38.
27 P.-E. Werner, L. Eriksson and M. Westdahl, *J. Appl. Crystallogr.*, 1985, **18**, 367–370.
28 P. I. Ravikovitch and A. V. Neimark, *Colloids Surf., A*, 2001, **187–188**, 11–21.
29 J. Jagiello and M. Thommes, *Carbon*, 2004, **42**, 1227.
30 H. V. R. Dias and H.-L. Lu, *Inorg. Chem.*, 1995, **34**, 5380–5382.
31 H. V. R. Dias and H.-J. Kim, *Organometallics*, 1996, **15**, 5374–5379.
32 K. Fujisawa, T. Ono, Y. Ishikawa, N. Amir, Y. Miyashita, K. Okamoto and N. Lehnert, *Inorg. Chem.*, 2006, **45**, 1698–1713.
33 (*a*) N. Armaroli, G. Accorsi, F. Cardinali and A. Listorti, in *Curr Chem*, ed. V. Balzani and S. Campagna, Springer-Verlag, Berlin Heidelberg, Germany, 2007, vol. 280, pp. 69–115; (*b*) P. C. Ford, W. Cariati and J. Bourassa, *Chem. Rev.*, 1999, **99**, 3625.
34 (*a*) Y.-N. Gong, L. Jiang and T.-B. Lu, *Chem. Commun.*, 2013, **49**, 11113–11115; (*b*) B. Gole, A. K. Bar and P. S. Mukherjee, *Chem. – Eur. J.*, 2014, **47**, 12137–12139; (*c*) S.-R. Zhang, D.-Y. Du, J.-S. Qin, S.-J. Bao, S.-L. Li, W.-W. He, Y.-Q. Lan, P. Shen and Z.-M. Su, *Chem. – Eur. J.*, 2014, **20**, 3589–3594; (*d*) S. L. Jackson, A. Rananaware, C. Rix, S. V. Bhosale and K. Latham, *Cryst. Growth Des.*, 2016, **16**, 3067–3071.
35 A. Dhakshinamoorthy, A. M. Asiri and H. García, *Angew. Chem., Int. Ed.*, 2016, **55**, 5414–5445.
36 M. I. Rodriguez-Franco, I. Dorronsoro, A. I. Hernández-Higueras and G. Antequera, *Tetrahedron Lett.*, 2001, **42**, 863–865.
37 *APEX2 Version 2011.6*, Bruker AXS Inc.
38 *SAINT Version 8.32B*, Bruker AXS Inc., 2013.
39 XL Version 2013/3: G. M. Sheldrick, *Acta Crystallogr., Sect. A: Fundam. Crystallogr.*, 2008, **64**, 112.
40 U. Mueller, N. Darowski, M. R. Fuchs, R. Forster, M. Hellmig, K. S. Paithankar, S. Puhringer, M. Steffien, G. Zocher and M. S. Weiss, *J. Synchrotron Radiat.*, 2012, **19**, 442–449.
41 W. Kabsch, *J. Appl. Crystallogr.*, 1988, **21**, 67.
42 G. M. Sheldrick, *Acta Crystallogr., Sect. C: Cryst. Struct. Commun.*, 2015, **71**, 3–8.